Carbohydrate Polymers 93 (2013) 122–128

Contents lists available at SciVerse ScienceDirect

Carbohydrate Polymers

journal homepage: www.elsevier.com/locate/carbpol

Novel insight into cellulose supramolecular structure through ^{13}C CP-MAS NMR spectroscopy and paramagnetic relaxation enhancement

Gerhard Zuckerstätter[a], Nicoleta Terinte[b], Herbert Sixta[c], Kurt Christian Schuster[b,*]

[a] Kompetenzzentrum Holz GmbH, St.-Peter-Strasse 25, 4021 Linz, Austria
[b] Lenzing AG, Werkstrasse 2, 4860 Lenzing, Austria
[c] Helsinki University of Technology, Vourimiehentie 1, 02015 Espoo, Finland

ARTICLE INFO

Article history:
Received 6 December 2011
Received in revised form 22 March 2012
Accepted 4 May 2012
Available online 17 May 2012

Keywords:
Cellulose I
Cellulose II
^{13}C CP-MAS NMR
Paramagnetic relaxation enhancement
Spectral fitting
Lateral crystallite dimensions

ABSTRACT

^{13}C CP-MAS NMR and paramagnetic relaxation enhancement provide novel insight into the supramolecular structure of solid cellulose I and II. Separable NMR signals associated with crystalline interiors, solvent accessible and inaccessible surfaces, as well as non-crystalline material are assigned and confirmed. For the first time solvent accessibility is evidenced and monitored through ^{13}C T_1 NMR relaxation enhancement in paramagnetic medium. Established NMR signal assignments for cellulose I have been confirmed. Existing cellulose II resonance attributions have been modified and extended. Novel spectral fitting routines for cellulose II allow for the reproducible quantification of separable signal contributions. Results from NMR line shape analyses are straightforwardly introduced into a model for cellulose II supramolecular structure.

1. Introduction

Cellulose is a technically important and fascinating biopolymer, as well as an almost inexhaustible natural resource. The renewable material is a major component of the cell walls of higher plants, e.g. wood and cotton, and is also produced by some bacteria, algae, fungi and sea-animals. Cellulose typically exhibits a relatively high degree of order, i.e. crystallinity. Several crystalline forms are known today (Zugenmaier, 2001). Native cellulose, however, is always cellulose I. Cellulose II can also be formed through alkalization and regeneration. Some of the numerous uses of cellulose II include textile fibres and films. Cellulose I is also an important component in the paper, paperboard and textile industry, chemical technology and construction. Native and regenerated cellulose fibres are both further used as medical and sanitary materials. Chemically, cellulose can also be transformed into several derivatives, e.g. cellulose acetate, carboxymethyl cellulose and many more.

For several decades considerable attention has been paid on an enhanced understanding of cellulose supramolecular structure. The latter has been found to relate strongly to cellulose materials chemical and physical properties. The chemical reactivity of a cellulose material is mainly governed by its overall accessibility towards solvents and reactants. Less ordered inter-crystalline domains as well as crystallite surfaces are highly susceptible to interactions with reactants. Non-penetrated crystallite cores are, however, largely chemically stable. The arrangement of crystalline fibrils into fibril aggregates has been shown to further impact on the chemical reactivity of cellulose I (Chunilall, Bush, Larsson, Iversen, & Kindness, 2010). Chemical treatment, e.g. cold caustic extraction (CCE), can lead to enlarged fibril aggregates and thus reduced solvent accessibility (Wollboldt, Zuckerstätter, Weber, Larsson, & Sixta, 2010). Similar effects are also observed upon thermal treatment of pulp ("hornification"). The physical properties of cellulose materials, such as density and tensile strength, are influenced by such ultra-structural changes as well. In regenerated cellulose (cellulose II) textile fibres, treatments with caustic agents introduce changes in macroscopic properties like tenacity and dye uptake, which can be related to ultrastructural changes like crystallinity, crystallite dimensions, and porosity (Öztürk et al., 2009).

Solid-state nuclear magnetic resonance (NMR) spectroscopy has been used extensively to study the supramolecular structure of cellulose materials. Larsson, Wickholm, and Iversen (1997) have analysed Zuckerstätter et al. (2009) complex cellulose I ^{13}C CP-MAS NMR resonances through spectral fitting. Separated signal contributions have been attributed to crystalline interiors, as well as accessible and inaccessible fibril surfaces (Wickholm, Larsson, & Iversen, 1998). From the relative amounts of these components,

* Corresponding author.
E-mail address: c.schuster@lenzing.com (K.C. Schuster).

0144-8617/$ – see front matter © 2012 Elsevier Ltd. All rights reserved.
http://dx.doi.org/10.1016/j.carbpol.2012.05.019

lateral fibril and fibril aggregate dimensions have been computed. These NMR derived dimensions corroborate with those obtained by electron microscopy (Duchesne et al., 2001). For cellulose II; the assignment of ^{13}C CP-MAS NMR signals to the carbons C1, C4, C2-3-5 and C6 has been studied in detail by Kono, Numata, Erata, and Takai (2004). They obviously used a very highly crystalline material where the C4 signal consisted only of two peaks. They discussed that the dubletts observed for each carbon signal arises either from the existence of two distinct chains with different glycosidic bond angles, or from the hydroxymethyl group at C6 having either *tg* or *gt* conformation in equal distribution. Newman and Davidson (2004) have assigned the fine structure in the C4 resonances of semicrystalline cellulose II materials associated to inner-crystalline, surface crystalline and non-crystalline (also termed disordered) cellulose II material. Further information on cellulose II signal assignment was provided by Ibbett, Domvoglou, and Fasching (2007) and Ibbett, Domvoglou, Wortmann, and Schuster (2010) who have analysed hydrolysed regenerated cellulose fibres in a dry state using signal-deconvolution and spin relaxation editing experiments.

Here, we present novel insight into cellulose I and II supramolecular structure through ^{13}C CP-MAS NMR spectroscopy. Physical evidence is presented that both cellulose I and II materials exhibit separable NMR signals for crystallite cores and surfaces. This is attained through a mechanism called paramagnetic relaxation enhancement (PRE). Furthermore, we show enhanced cellulose II spectral assignments, spectral fitting routines, and a model for cellulose II ultrastructure.

2. Materials and methods

In this study the ^{13}C CP-MAS NMR spectral features of cellulose I and II samples were investigated. One commercial ENCE pulp (Wollboldt et al., 2010) was selected as an example of cellulose I. Regenerated cellulose fibres of the Lyocell generic type produced with the cellulose/NMMO/water system (brand names: Lenzing Lyocell® and TENCEL®) were kindly supplied by Lenzing AG, Austria as an example of cellulose II. In this work Lyocell fibres with an average linear density of 1.3 dtex (0.13 g/1000 m) were coarsely ground to pass a 0.5 mm sieve. One Lyocell sample and all ENCE pulp samples have been subjected to acid hydrolysis in 2.5 M HCl at 80 °C for 2 h.

3. Experimental

Approximately 150 mg of air-dry pulp or coarsely ground cellulose II fibre were placed into 2 ml Eppendorf tubes and soaked with 1.5–2 ml deionised water for at least half a day. For the PRE measurements 30–35 mg 4-hydroxy-2,2,6,6-tetramethylpiperidin-1-oxyl (4-OH-TEMPO, 97.0%, CAS-No.: 2226-96-2, as purchased from Sigma–Aldrich) were added to the sample tubes. After equilibration the soaked cellulose samples were packed tightly into 4 mm outer diameter zirconium oxide magic angle spinning (MAS) rotors.

Solid-state ^{13}C CP-MAS NMR analyses were conducted on a Bruker Avance DPX300 NMR spectrometer, operating at 75 MHz ^{13}C NMR resonance frequency. The spectrometer was equipped with a 4 mm Bruker MAS probe and samples were spun at 4 kHz MAS speed. ^{13}C CP-MAS and ^{13}C longitudinal relaxation (T_1) CP-MAS (Torchia, 1978) NMR measurements were performed at room temperature with the following acquisition parameters: cross-polarization (CP) contact time 1 ms, repetition interval 3 s, acquisition time 41 ms, SPINAL-64 ^{1}H decoupling, at least 2048 accumulations per T_1 increment or CP-MAS spectrum. T_1 delays have been varied from 0.001 s to 10 s, and also up to 100 s for selected experiments. Chemical shifts were referenced externally against glycine (δ ^{13}C = 176.03 ppm for the carbonyl signal). The acquired free inductions decays (FIDs) were Fourier transformed without apodization.

^{13}C CP-MAS and ^{13}C T_1 CP-MAS NMR spectra were processed and analysed with the TopSpin 1.3, 2.1 and 3.1 software, as provided by the instrument manufacturer. All ^{13}C CP-MAS spectra and slices from ^{13}C T_1 CP-MAS NMR experiments were analysed with the Solver tool in Microsoft Excel spreadsheets. Spectral fitting was achieved mainly by variation of individual signal intensities. Line widths were found to depend mainly with the type of investigated cellulose substrate and NMR experimental set-up. Signal positions were held constant in all spectral fittings.

4. Results and discussion

^{13}C CP-MAS NMR spectra of wetted cellulose I and II exhibit numerous separable resonance lines (Fig. 1). One particularly well resolved and highly dispersed signal complex is that associated to the anhydroglucose unit (AGU) C4 carbon atom. Detailed assignments of C4 signal contributions have been published for cellulose I and II (Ibbett et al., 2007; Larsson et al., 1997; Newman & Davidson, 2004; Wickholm et al., 1998). For cellulose I Larsson et al. (1997) have introduced spectral fitting routines that separate crystalline and paracrystalline resonances, as well as signals assigned to fibril surfaces. Wickholm et al. (1998) have presented more detailed assignments of non-crystalline contributions. The rational for their assignments of accessible and inaccessible fibril surfaces have been based on ^{13}C T_1 NMR relaxation data and acid hydrolysis experiments. Relatively short longitudinal relaxation times of two sharp NMR signals at 84.2 and 83.2 ppm have been interpreted in terms of increased mobility due to intimate contact with solvent water. The broad resonance centred at ca. 83.9 ppm has been found to be largely unaffected by acid hydrolysis and has thus been considered a solvent-inaccessible surface structure. However, unambiguous spectroscopic evidence for the attribution of solvent accessible crystal surfaces has been missing.

Surface crystalline signal contributions have also been identified for cellulose II. Newman and Davidson (2004) have assigned one inner-crystalline signal, one overlapping resonance of inner-crystalline and surface-crystalline material, as well as one surface

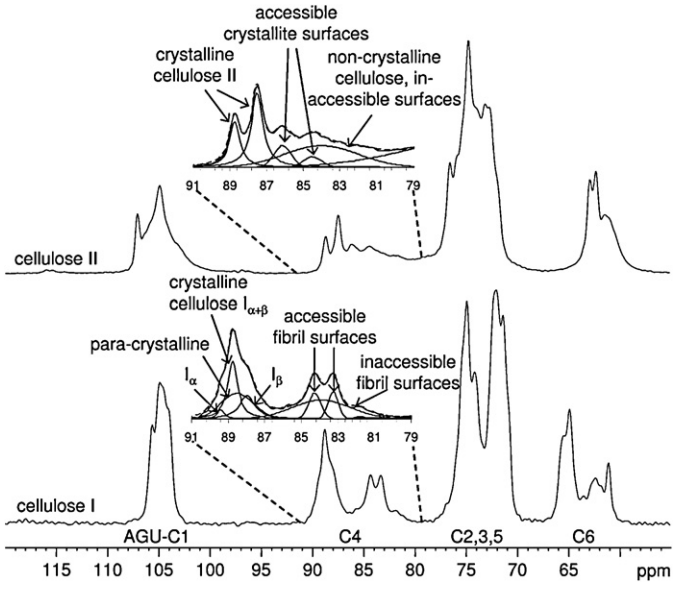

Fig. 1. ^{13}C CP-MAS NMR spectra of cellulose I (bottom) and cellulose II (top). Note the highly dispersed and splitted AGU-C4 and C6 resonances in both spectra. Spectral fitting routines can be used to analyse e.g. the cellulose I and II AGU-C4 signals domains as shown in the inserts on top of both spectra.

and one broad non-crystalline contribution. Ibbett et al. (2007) have followed their assignations, confirmed them by spin relaxation editing experiments, and introduced a peak deconvolution of four peaks, for crystalline (two peaks at 89.5 and 88.3 ppm), partly ordered or surface crystalline (one peak at 86.8 ppm) and fully disordered material (a broad peak at 83.2 ppm). This deconvolution allowed for a quantitative estimation of the respective structure components in hydrolysed regenerated cellulose fibres in a dry state (Ibbett et al., 2010). Our ^{13}C CP-MAS NMR analyses on wet cellulose II materials exhibiting intense surface crystalline contributions brought forth another sharp signal centred at 84.5 ppm (Fig. 1, top). This resonance has not been observed in previous studies. Our tentative assignment was that of another surface crystalline contribution, as has also been suggested by molecular dynamics computations (Newman & Davidson, 2004). Further, we have noted one signal centred at ca. 81.7 ppm, which has been attributed to short chain celluloses and/or xylan.

Spectral fitting routines for cellulose II materials have been established, which use the following contributions: two Lorentzian lines centred at 88.7 (full width at half maximum FWHM = 51 Hz) and 87.5 ppm (FWHM = 57 Hz), two narrow Gaussian lines at 86.1 (FWHM = 84 Hz) and 84.5 ppm (FWHM = 89 Hz), one broad Gaussian line at 83.9 ppm (FWHM = 338 Hz) and one Gaussian line at 81.7 ppm (FWHM = 89 Hz). Further the tail of the neighbouring C2,3,5 signal complex was fitted in the spectral analysis. Note here, that in several instances signal splitting of both resonances at 86.1 ppm and at 84.5 ppm into doublets has been observed. Typical peak positions are then 86.37 and 85.82 ppm as well as 84.65 and 84.21 ppm for both surface crystalline contributions. Note here, that resonance positions cited in the literature may vary significantly from ours, due to different chemical shift referencing.

4.1. Paramagnetic relaxation enhancement (PRE)

A novel approach to confirm solvent accessible crystallite surface signals is proposed using PRE NMR experiments in the solid state (Linser, Chevelkov, Diehl, & Reif, 2007; Solomon, 1955). This technique was also previously used for chemical shift assignments and structure elucidation of proteins mainly in the liquid-state (Gillespie & Shortle, 1997; Pintacuda & Otting, 2002). Paramagnetic ions or radicals lead to faster (i.e. enhanced) relaxation of spins near to the paramagnetic centre. This effect can be detected over relatively large distances up to ca. 15–25 Å (1.5–2.5 nm). In the liquid state PRE therefore mainly provides long-range distance information and is detected via increased transverse relaxation rates. In this study, we utilised the increased solid state longitudinal (T_1) relaxation rates near to a paramagnetic radical. We employed the stable and water soluble paramagnetic nitroxyl radical 4-OH-TEMPO in our NMR experiments. 4-OH-TEMPO is distributed within the cellulose material through soaking in doped aqueous solution. Solvent accessible regions of the cellulose material are then expected to exhibit a higher radical concentration than inner-crystalline regions. Consequently, solvent accessible crystallite surfaces experience a stronger relaxation enhancement than the crystallite cores and inaccessible crystallite surfaces (Fig. 2).

In ^{13}C T_1 CP-MAS NMR experiments (Torchia, 1978) a delay t during the pulse sequence is varied, where a given NMR signal is attenuated through spin–lattice relaxation T_1. With increasing relaxation delay times t exponential signal decay with a rate constant t/T_1 is observed. Typically, signals associated to highly ordered material, e.g. crystallite interiors, decay much slower than those assigned to non-crystalline or solvent accessible material due to restricted local mobility. The enhancement of longitudinal relaxation times T_1 through addition of a paramagnetic dope can be monitored from analysing decay curves with and without added dope (Fig. 3). Largest deviations upon 4-OH-TEMPO addition

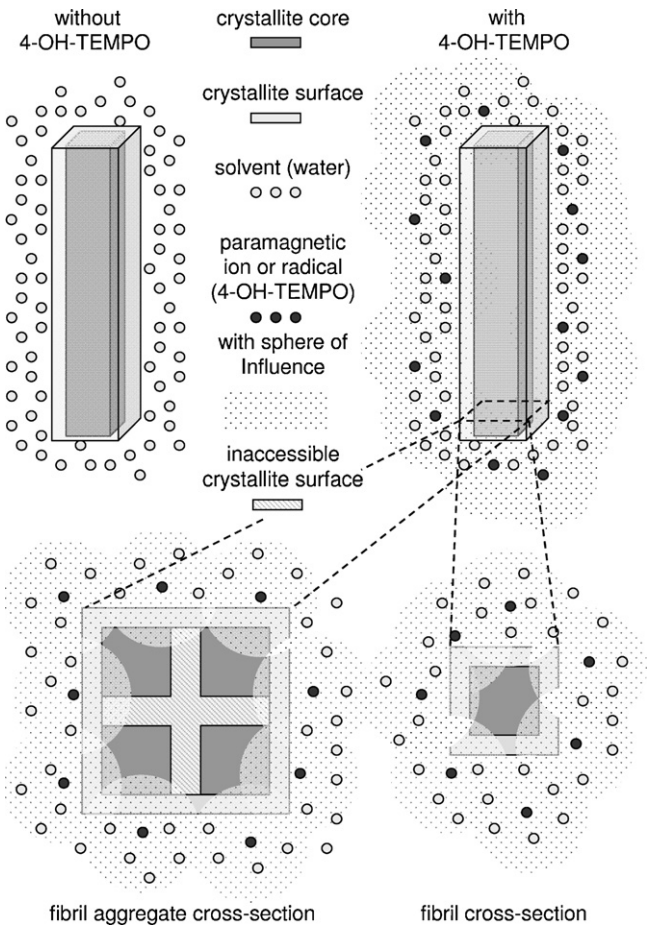

Fig. 2. Concept of paramagnetic relaxation enhancement (PRE) used to study the solvent accessibility of different fractions of wetted cellulose. Material located inside the spheres of influence of paramagnetic 4-OH-TEMPO radicals exhibit dramatically increased longitudinal relaxation rates. Signal contributions associated with accessible crystallite surfaces are expected to show the strongest PRE, while crystalline interiors and in particular inaccessible fibril surfaces (if present) are expected to experience less enhancement.

indicate most intense contact with the surrounding solvent. Due to the relatively large sphere of influence of 4-OH-TEMPO compared to the small crystallite and fibril dimensions, all cellulose signals are attenuated to some degree, however. The overall relaxation enhancement of a given resonance is also dependent on the concentration of the paramagnetic dope. Here, relatively high concentrations of 4-OH-TEMPO (ca. 0.1 mol/l) have been used to observe a strong PRE effect.

For cellulose I a strong PRE effect was observed (Table 1). ^{13}C T_1 relaxations times for accessible fibril surfaces signals at 84.2 and 83.2 ppm have decreased from 15.6 s to only 0.7 s upon 4-OH-TEMPO addition (−2229%). Crystalline interiors and in particular inaccessible fibril surfaces experience significantly less relative enhancement. These results corroborate with the model of aggregates of coaxial crystalline fibrils as proposed by Wickholm et al. (1998) (Fig. 2, bottom left).

PREs of cellulose II ^{13}C CP-MAS NMR resonances appear somewhat more uniform than those of cellulose I. Still, we observe the most pronounced PRE effect for tentatively assigned accessible crystallite surface signals at 86.1 and 84.5 ppm (Fig. 3, right). The magnitude of PRE is, however, considerably lower than that observed for cellulose I (Table 1), which is also attributed to imperfect distribution of 4-OH-TEMPO within the coarsely ground fibre. This conjecture is supported by the fact that the decay curves of cellulose II wetted with doped water exhibit no single exponential

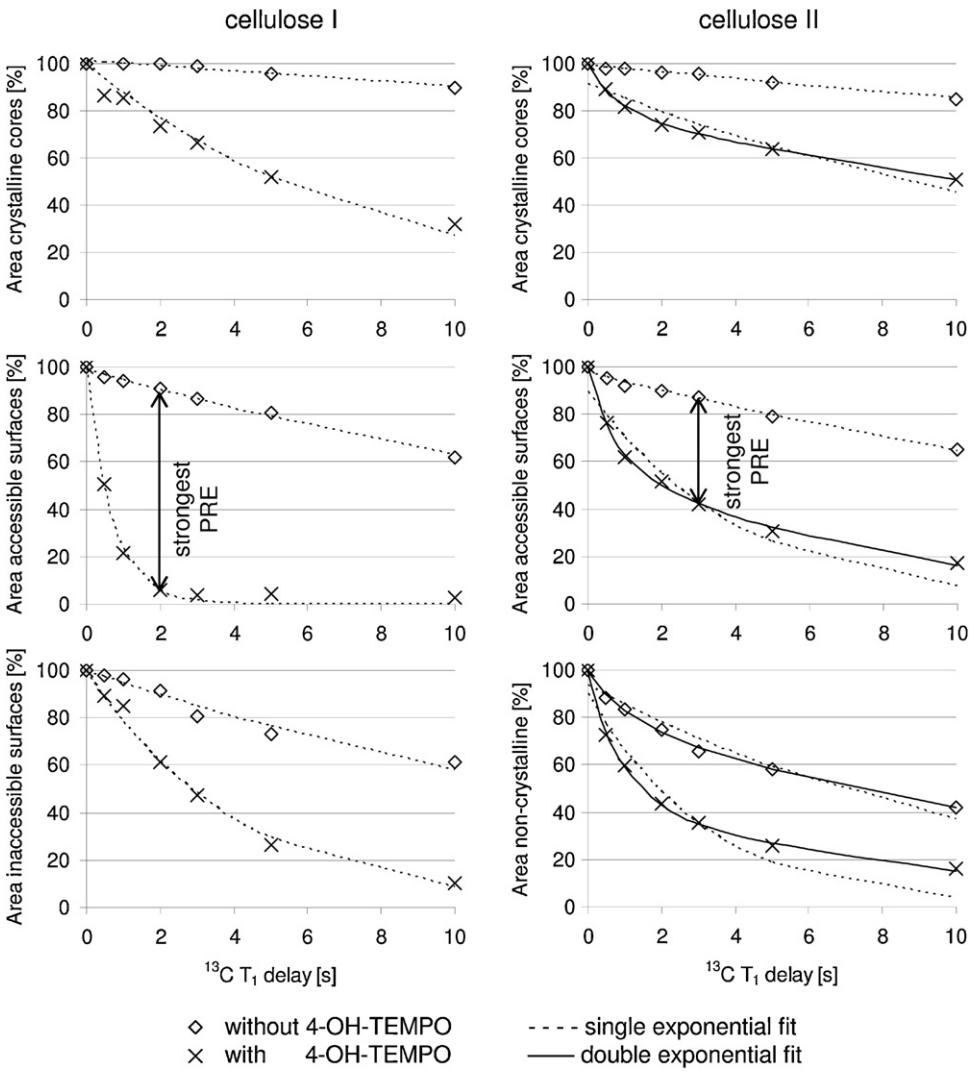

Fig. 3. Relaxation decay curves obtained from ^{13}C T$_1$ CP-MAS NMR experiments on cellulose I (left) and cellulose II (right) without (diamonds) and with (squares) addition of paramagnetic 4-OH-TEMPO. The indicated areas of the respective resonance contributions have been determined by spectral fitting of individual relaxation delay *t* increments. All signal contributions have been normalised to an initial (*t* = 0 s) value of 100%. Note the strong PRE effect observed for accessible fibril surfaces and crystallite surfaces in cellulose I and II, respectively. For cellulose II the area of the non-crystalline contribution includes inaccessible crystallite surfaces.

Table 1
Cellulose I and II paramagnetic relaxation enhancements (PRE).

Cellulose I				
Assignment	Signal contributions δ [^{13}C, ppm]	^{13}C T$_1$ [s] without 4-OH-TEMPO	^{13}C T$_1$ [s] with 4-OH-TEMPO	PRE [%]
Crystalline cores	89.4, 88.8, 88.5, 88.0	103.9	7.6	1361
Accessible fibril surfaces	84.2, 83.2	15.6	0.7	2229
Inaccessible fibril surfaces	83.9	19.4	4.1	470

Cellulose II				
Assignment	Signal contributions δ [^{13}C, ppm]	^{13}C T$_1$ [s] without 4-OH-TEMPO	^{13}C $T_{1a,b}$ [s] with 4-OH-TEMPO[a]	PRE [%]
Crystalline cores	88.7, 87.5	64.8	0.8 (T_{1a}) (20% $I_{0,a}$)	–
			21.8 (T_{1b}) (80% $I_{0,b}$)	–
			17.6 (wt. average)	367
Accessible crystallite surfaces	86.1, 84.5	24.1	0.6 (T_{1a}) (37% $I_{0,a}$)	–
			7.4 (T_{1b}) (63% $I_{0,b}$)	–
			4.9 (wt. average)	493
Non-crystalline material and inaccessible surfaces	84.0	12.1	0.9 (T_{1a}) (53% $I_{0,a}$)	–
			8.9 (T_{1b}) (47% $I_{0,b}$)	–
			4.6 (wt. average)	261

[a] Double exponential behaviour observed: fast relaxing component a; slowly relaxing component b.

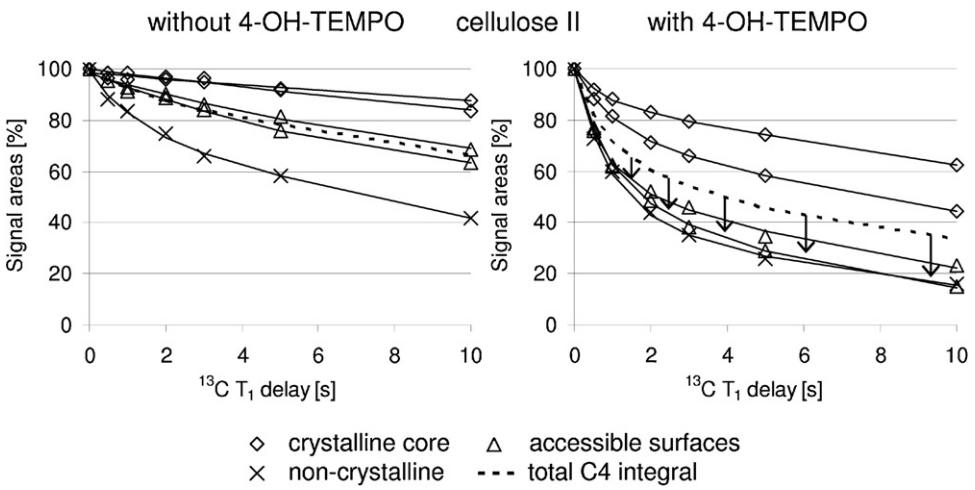

Fig. 4. ^{13}C T_1 relaxation decay curves for five signal components in cellulose II ^{13}C CP-MAS NMR spectra. The cellulose material has been soaked in water (left) and in paramagnetic 4-OH-TEMPO solution (right) prior to analysis. Note, that both inner-crystalline and both surface-crystalline signal components exhibit very similar relaxational properties, when the sample is wetted with water (left). Upon addition of a paramagnetic dope crystallite surfaces experience much stronger PRE than the sum of all AGU-C4 contributions. Note further, that both inner-crystalline signals experience differential relaxation enhancement.

behaviour (see dotted lines in Fig. 3, right). Instead, biexponential relaxation behaviour is suggested from visual inspection. Similar behaviour has been described for other polymers in the literature (Lin, Zhang, Yang, & Chen, 2003) as well. Here, a quickly relaxing component attributes to the sharp initial signal decline, while the slowly relaxing component contributes to the flat tail of the curve. Quickly and slowly relaxing components are assigned to cellulose II in close contact with 4-OH-TEMPO radicals and cellulose II in locally less- or un-doped environment. Consequently, we observe a parallel course of relaxation curves for doped and undoped cellulose II for >2–3 s relaxation interval. Biexponential fittings of experimental ^{13}C T_1 decay curves have been attempted with a function of the form:

$$I(t) = I_{0,a} \cdot e^{-t/T_{1,a}} + I_{0,b} \cdot e^{-t/T_{1,b}} \quad (1)$$

Here, $T_{1,a}$ and $T_{1,b}$ are two independent spin–lattice relaxation times. $I_{0,a}$ and $I_{0,b}$ can be considered as weighting factors for both differentially relaxing components. It is evident, that biexponential fitting of only seven datapoints could lead to ambiguous results. However, we have attained very similar results for repeated analyses and numerous different starting values used for the fitting procedure. We therefore conclude the usefulness of such a fitting in this particular case.

Quickly relaxing components of all signal contributions exhibit ^{13}C T_1 times in the order of less than 1 s. However, for cellulose located at solvent accessible crystallite surfaces and the non-crystalline fraction, the fast relaxing components (frc) attribute to 37% and 53% ($I_{0,frc}$) of the material, respectively. In contrast to that only 20% of the inner-crystalline material is in close contact with 4-OH-TEMPO and is thus relaxing quickly (Table 1). This supports our assumption, that non-crystalline material is also highly solvent accessible. Interestingly, the tentatively assigned non-crystalline resonance exhibits double exponential behaviour also when wetted with pure water. This indicates the presence of two overlapping contributions, one non-crystalline and one associated with inaccessible crystallite surfaces (see Section 4.2) (Krässig, 1993). Further support for this assignment is given by the relative PRE magnitudes, which are similar to that observed for cellulose I (Table 1).

Relaxation decay curves for five individual signal components as observed in cellulose II ^{13}C CP-MAS NMR spectra are shown in Fig. 4. When wetted with water, both inner-crystalline contributions exhibit very similar relaxation profiles. This indicates that both resonances are associated to the same crystal lattice. Moreover, the signal at 87.5 ppm shows a single exponential relaxation decay profile with no perceptible overlap from a fast relaxing surface crystalline contribution. This contrasts the previous assignment by Newman and Davidson (2004), where the peak at 87.5 ppm was assigned a mixed surface plus inner-crystalline contribution. Both surface crystalline resonances at 86.1 and 84.5 ppm again exhibit similar relaxation behaviour. This is different to the findings on cellulose I by Bergenstråhle, Wohlert, Larsson, Mazeau, and Berglund (2008), where two different crystal faces with relaxation times differing in a factor 2 were found experimentally and by molecular modelling. Upon addition of 4-OH-TEMPO longitudinal relaxation rates of these components are enhanced much more than the average of all signals (Fig. 4). This again demonstrates the pronounced solvent accessibility of the associated surface crystalline material.

Addition of the paramagnetic reagent further enhances the relaxation of one inner-crystalline contribution significantly more than that of the other. This may be interpreted in terms of differential proximity of corner and centre chains (Zugenmaier, 2001) in cellulose II crystals with respect to the surrounding solvent. Another possible interpretation is a preferred adsorption of the TEMPO molecule to the more hydrophobic crystal surface, analogous to the observations by Mazeau and Vergelati (2002) on the adsorption of benzophenon on cellulose I surfaces. The crystal surface signals show only a slight difference in relaxation behaviour.

4.2. Cellulose II supramolecular structure

The solvent accessibility of non-crystalline material has further been confirmed by acid hydrolysis experiments (Wickholm et al., 1998). In Fig. 5 ^{13}C CP-MAS NMR spectra of the same coarsely ground Lyocell fibre before and after mild acid hydrolysis are depicted. A major fraction of tentatively assigned non-crystalline material is removed by the treatment. For less crystalline materials such as viscose fibres (results not shown) the effect of acid hydrolysis is even much clearer than for highly crystalline Lyocell fibre. However, even after prolonged hydrolysis a broad Gaussian peak centred at ca. 83.9 ppm is detected in ^{13}C CP-MAS NMR spectra. This corroborates with an additional, major contribution from inaccessible crystallite surfaces, which are resistant against mild acid hydrolysis. The assignment of inaccessible surfaces evidences the presence of crystallite aggregates, as has been suggested by Krässig (1993).

Table 2
Quantitative evaluation of Lyocell ^{13}C CP-MAS NMR spectra.

Signal assignment	Signal fraction [%] non-hydrolysed fibre	Signal fraction [%] hydrolysed fibre
Crystalline cores	44.2	57.4
Accessible fibril surfaces	13.8	13.5
Inaccessible fibril surfaces/non-crystalline material	42.0	29.1
Computed parameters	**Lateral dimensions non-hydrolysed fibre [nm]**	**Lateral dimensions non-hydrolysed fibre [nm]**
Lateral fibril aggregate width LFAD (Chunilall et al., 2010)	15.9	16.3
Fibril width – aggregate model (Wickholm et al., 1998)	3.4	4.7
Fibril width – fibril model (Ibbett et al., 2010)	9.0	11.4
Fibril width – WAXD data taken from (Ibbett et al., 2010)	3.3	4.8[a]

[a] Hydrolysed with 1.0 M sulphuric acid (Ibbett et al., 2010).

From the above presented findings we have established a model for the supramolecular structure of cellulose II (Fig. 6). Similarly to cellulose I, crystallite aggregates are suggested also for cellulose II. Further, the cellulose II crystallite aggregates are proposed to be surrounded by solvent accessible non-crystalline material. Crystallite surfaces are assumed to be monomolecular layers of cellulose with a thickness of 0.57 nm and directly attached to the crystalline core. From the fractions q of surface-crystalline cellulose lateral dimensions (LD) of fibrils and fibril aggregates can be computed (Chunilall et al., 2010; Ibbett et al., 2010; Wickholm et al., 1998) (Table 2):

$$\mathrm{LD} = 0.57\ \mathrm{nm} \cdot \left(\frac{2 + \sqrt{4 - 4q}}{q} \right) \quad (2)$$

Assuming a fibril aggregate model (AM), $q_{\mathrm{fibril,AM}}$ is the fraction of accessible plus inaccessible fibril surfaces (as well as overlapping non-crystalline material), which yields estimates for lateral fibril dimensions (Wickholm et al., 1998). Lateral fibril aggregate dimensions (LFAD) (Chunilall et al., 2010) are computed using $q_{\mathrm{aggregate,AM}}$, which denotes the fraction of solvent accessible fibril surfaces only. For a simple fibrillar model (FM) (Ibbett et al., 2010), $q_{\mathrm{fibril,FM}}$ is the ratio of accessible surfaces versus accessible surfaces plus inner-crystalline material.

For non-hydrolysed Lyocell fibre we attain lateral fibril dimensions of 3.4 nm using a fibril aggregate model according to Chunilall et al. (2010). This corresponds nicely with lateral crystallite dimensions of 3.3 nm as derived from WAXD analyses (Ibbett et al., 2010).

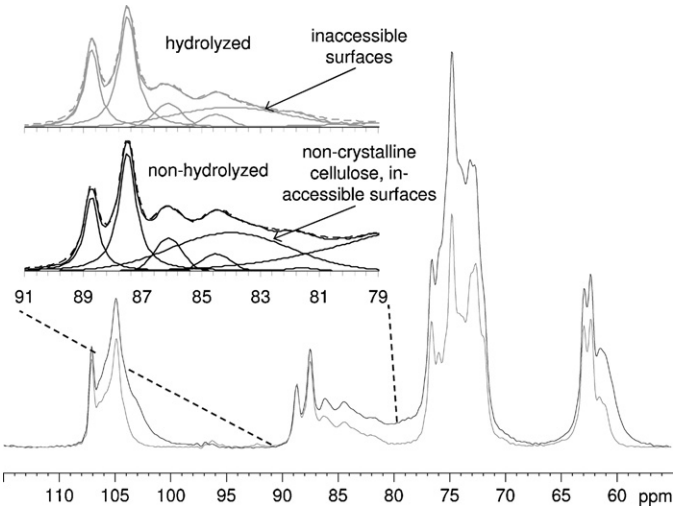

Fig. 5. Lyocell fibre before (black line, AGU-C4 spectral fitting below) and after acid hydrolysis (grey line, AGU-C4 spectral fitting on top). Note, that most non-crystalline cellulose has been removed, while inner-crystalline and surface-crystalline contributions remain largely unaffected.

In contrast, the simple fibrillar model yields a lateral fibril width of 9.0 nm. This disagrees with the values presented by Ibbett et al. (2010), who reported fibril dimensions close to that derived from WAXD. We attribute the differences in computed fibril widths mainly to differential spectral resolution in wet-state and dry-state analyses. Further the employed spectrometer hardware and decoupling, as well as spectral fitting routines impact strongly on analysis results.

Upon acid hydrolysis an increase in lateral fibril dimensions is observed. WAXD analyses (Ibbett et al., 2010) on hydrolysed Lyocell fibres yielded the same trend with similar quantitative results (Table 2). Ibbett, Domvoglou, and Phillips (2008) and Ibbett et al. (2010) attributed the increase in crystallite sizes to a partial re-crystallisation of non-crystalline material on the crystal surfaces during hydrolysis. However, the effect may also be attributed to erosion of smaller structural elements by hydrolysis, leading in this way to larger average dimensions. LFAD computations corroborate with this assumption and also agree with values reported by Krässig (1993). Aggregate widths remain largely constant at a level of about 16 nm before and after mild acid hydrolysis. This is consistent with crystal growth at a concomitant decrease in the number of fibrils forming an aggregate during hydrolysis.

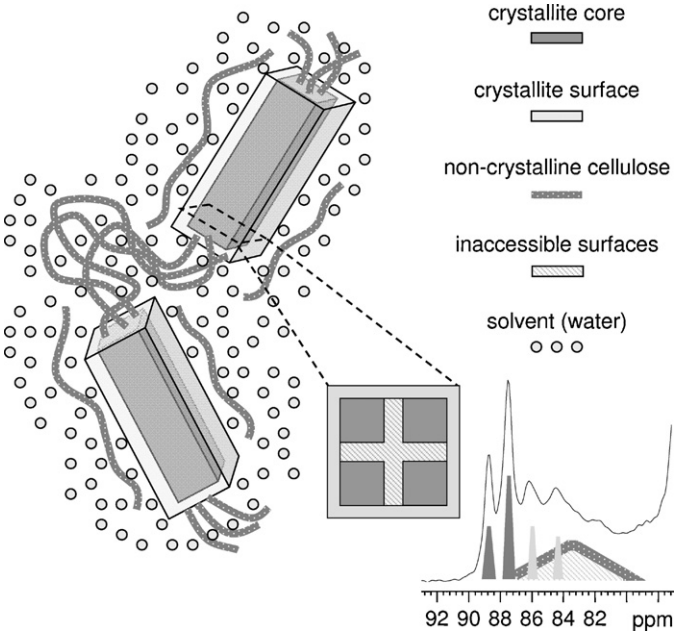

Fig. 6. Suggested model for cellulose II supramolecular structure according to ^{13}C CP-MAS NMR, PRE and acid hydrolysis experiments. From spectral fitting the relative amounts of crystalline cores, solvent accessible and inaccessible surfaces can be derived. Under the assumption of a monomolecular layer of accessible crystallite surfaces and square fibril cross-sections, lateral fibril and fibril aggregate dimensions can be computed.

5. Conclusions

Paramagnetic relaxation enhancement (PRE) studies on solid cellulose I and II provide novel insight into the assignment of their complex ^{13}C CP-MAS NMR spectra. We have shown that the ^{13}C T_1 NMR relaxation rates of solvent accessible regions in water-soaked cellulose are strongly enhanced upon addition of a paramagnetic reagent. The established assignments of solvent accessible and inaccessible fibril surfaces signals in cellulose I have therefore been confirmed. Existing NMR signal assignments for cellulose II have been modified and extended with a previously undiscovered surface crystalline resonance. Separable spectral contributions for crystallite cores, accessible and inaccessible surfaces, as well as solvent accessible non-crystalline cellulose have been identified. Acid hydrolysis experiments have shown that non-crystalline fractions of cellulose II samples are solvent accessible and easily removed. Based on our experiments a model for cellulose II supramolecular structure with fibril aggregates has been established. A spectral fitting routine for the AGU-C4 region in cellulose II ^{13}C CP-MAS NMR spectra has been presented. Results from line shape analyses were used to compute plausible lateral fibril and fibril aggregate dimensions for cellulose II.

Acknowledgements

The European Union's Seventh Framework Program [FP7/2007-2013] financially supported the present research as part of the STEP ITN Project (grant agreement no. 214015).

References

Bergenstråhle, M., Wohlert, J., Larsson, P. T., Mazeau, K., & Berglund, L. (2008). Dynamics of cellulose–water interfaces: NMR spin–lattice relaxation times calculated from atomistic computer simulations. *Journal of Physical Chemistry B*, *112*(9), 2590–2595.

Chunilall, V., Bush, T., Larsson, P. T., Iversen, T., & Kindness, A. (2010). A CP/MAS ^{13}C NMR study of cellulose fibril aggregation in eucalyptus dissolving pulps during drying and the correlation between aggregate dimensions and chemical reactivity. *Holzforschung*, *64*, 693–698.

Duchesne, I., Hult, E., Molin, U., Daniel, G., Iversen, T., & Lennholm, H. (2001). The influence of hemicellulose on fibril aggregation of kraft pulp fibres as revealed by FE-SEM and CP/MAS ^{13}C NMR. *Cellulose*, *8*, 103–111.

Gillespie, J. R., & Shortle, D. (1997). Characterization of long-range structure in the denatured state of staphylococcal nuclease. I: Paramagnetic relaxation enhancement by nitroxide spin labels. *Journal of Molecular Biology*, *268*, 158–169.

Ibbett, R., Domvoglou, D., & Fasching, M. (2007). Characterisation of the supramolecular structure of chemically and physically modified regenerated cellulosic fibres by means of high-resolution carbon-13 solid-state NMR. *Polymer*, *48*, 1287–1296.

Ibbett, R., Domvoglou, D., & Phillips, D. A. S. (2008). The hydrolysis and recrystallisation of lyocell and comparative cellulosic fibres in solutions of mineral acid. *Cellulose*, *15*, 241–254.

Ibbett, R., Domvoglou, D., Wortmann, F., & Schuster, K. C. (2010). Carbon-13 solid state NMR investigation and modelling of the morphological reorganization in regenerated cellulose fibres induced by controlled acid hydrolysis. *Cellulose*, *17*, 231–243.

Kono, H., Numata, Y., Erata, T., & Takai, M. (2004). ^{13}C and ^{1}H resonance assignment of mercerized cellulose II by two-dimensional MAS NMR spectroscopies. *Macromolecules*, *37*, 5310–5316.

Krässig, H. A. (1993). *Cellulose: Structure, accessibility and reactivity*. South Africa: Gordon and Breach Science Publishers., ISBN 2-88124-798-9.

Larsson, P. T., Wickholm, K., & Iversen, T. (1997). A CP/MAS ^{13}C NMR investigation of molecular ordering in celluloses. *Carbohydrate Research*, *302*, 19–25.

Lin, W., Zhang, Q., Yang, G., & Chen, Q. (2003). Biexponential ^{13}C spin–lattice relaxation behavior of the crystalline region of ethylene copolymers and its origin. *Journal of Molecular Structure*, *655*, 37–45.

Linser, R., Chevelkov, V., Diehl, A., & Reif, B. (2007). Sensitivity enhancement using paramagnetic relaxation in MAS solid-state NMR of perdeuterated proteins. *Journal of Magnetic Resonance*, *189*, 209–216.

Mazeau, K., & Vergelati, C. (2002). Atomistic modeling of the adsorption of benzophenone onto cellulosic surfaces. *Langmuir*, *18*, 1919–1927.

Newman, R. H., & Davidson, T. C. (2004). Molecular conformations at the cellulose–water interface. *Cellulose*, *11*, 23–32.

Öztürk, H. B., Potthast, A., Rosenau, T., Abu-Rous, M., MacNaughtan, B., Schuster, K. C., et al. (2009). Changes in the intra- and inter-fibrillar structure of Lyocell (TENCEL®) fibers caused by NaOH treatment. *Cellulose*, *16*, 37–52.

Pintacuda, G., & Otting, G. (2002). Identification of protein surfaces by NMR measurements with a paramagnetic Gd(III) chelate. *Journal of the American Chemical Society*, *124*, 372–373.

Solomon, I. (1955). Relaxation processes in a system of two spins. *Physical Review*, *99*, 559.

Torchia, D. A. (1978). The measurement of proton-enhanced carbon-13 T_1 values by a method which suppresses artifacts. *Journal of Magnetic Resonance*, *30*, 613–616.

Wickholm, K., Larsson, P. T., & Iversen, T. (1998). Assignment of non-crystalline forms in cellulose I by CP/MAS ^{13}C NMR spectroscopy. *Carbohydrate Research*, *312*, 123–129.

Wollboldt, R. P., Zuckerstätter, G., Weber, H. K., Larsson, P. T., & Sixta, H. (2010). Accessibility, reactivity and supramolecular structure of *E. globulus* pulps with reduced xylan content. *Wood Science and Technology*, *44*, 533–546.

Zuckerstätter, G., Schild, G., Wollboldt, P., Röder, T., Weber, H. K., & Sixta, H. (2009). The elucidation of cellulose supramolecular structure by ^{13}C CP-MAS NMR. *Lenzinger Berichte*, *87*, 38–46.

Zugenmaier, P. (2001). Conformation and packing of various crystalline cellulose fibers. *Progress in Polymer Science*, *26*, 1341–1417.